Title

Lullaby: A Novel Algorithm to Extract Fetal QRS in Real Time Using Periodic Trend Feature.

Journal

IEEE Sensors Letters, 6(9)

ISSN

2475-1472

Authors

Jilani, Daniel
Le, Tai
Etchells, Tim
et al.

Publication Date

2022-09-01

DOI

10.1109/lsens.2022.3200072

Peer reviewed

HHS Public Access

Author manuscript

IEEE Sens Lett. Author manuscript; available in PMC 2023 September 01.

Published in final edited form as:

IEEE Sens Lett. 2022 September ; 6(9): . doi:10.1109/lsens.2022.3200072.

Lullaby: A Novel Algorithm to Extract Fetal QRS in Real Time Using Periodic Trend Feature

Daniel Jilani[1,2], **Tai Le**[3], **Tim Etchells**[2], **Michael P.H. Lau**[2], **Hung Cao**[1,2,3]

[1]Department of Electrical Engineering, University of California Irvine, Irvine, CA 92697, USA

[2]Sensoriis, Inc., Edmonds, WA 98026, USA

[3]Department of Biomedical Engineering, University of California Irvine, Irvine, CA 92697, USA

Abstract

Fetal heart rate (fHR) is an important indicator for monitoring of fetal cardiac health and development. The widely-used method based on ultrasound, however, is not continuous and often requires an expert to perform; thus, it is mostly used in clinics during checkups. The advances in wearable technology have paved the way for home assessment of fHR via the extraction of the mother's abdominal electrocardiogram (ECG) acquired by novel patches. Several methods have been developed for such; however, the computation is either too slow for real-time monitoring or too heavy to be performed in a wearable. In this work, we develop and validate the Lullaby algorithm - a novel method for fetal QRS extraction from aECG. The results showed that Lullaby is almost 7 times faster than existing methods with a better F1-score of 0.815, holding promise to transform perinatal monitoring.

Keywords

Signal processing; biosignals; real-time; fetal heart rate (fHR); periodic trend feature (PTF); abdominal ECG (aECG); fetal QRS (fQRS)

I. INTRODUCTION

COVID-19 has incentivized the minimization of our interactions with others as the best protection against infection. Pregnant women are at the forefront of the most at-risk groups with higher likelihoods of hospitalization and death in contrast to non-pregnant women after COVID-19 infection according to the CDC [1]. While some medical services have been able to adapt using technologies that support telemedicine, but not as easily with regard to pregnancy. For pregnant women, certain services still require a clinical visit which creates a dilemma between guaranteeing the unborn child's wellbeing and risking COVID-19 related complications. Fetal heart rate (fHR) monitoring is one such service that currently requires a clinical visit. The service uses a Doppler ultrasound device to detect fetal heart beats which require a specialist to operate and interpret. fHR itself is an important indicator of fetal

Corresponding author: Hung Cao (hungcao@uci.edu).

wellbeing as it is commonly used to determine complications regarding fetal oxygenation, arrhythmia, and fetal acidosis [2].

Home-based fHR systems include over-the-counter Doppler-based and fetal ECG-based devices. The Doppler ones are simple and affordable, however, they are not easy to use and FDA issued a warning in 2014 on the repeating use of such [3]. ECG-based systems use the mother's abdominal electrocardiogram (aECG) to extract fHR or fQRS[4], [5]. These systems are somewhat unreliable because they either employ algorithms that are not simple enough to compute in real-time or cannot be computed directly on wearable devices [4], [5]. Real-time analysis of fHR is critical for life-saving intervention. Computation on the wearable device is free unlike fee-based high-end computing systems and negates latency issues associated with WiFi communication. Currently, the most common algorithms used for fQRS extraction are template subtraction (TS), Independent Component Analysis (ICA), and Extended Kalman Filtering (EKF). ICA is a method of extracting independent signal components from a multivariate signal. ICA is applied to the aECG signal and separates the aECG into the mECG, noise, and fetal ECG (fECG) components from which the fQRS are extracted [6]. Template Subtraction (TS) estimates the mECG component of the aECG and subtracts the estimated mECG from the aECG to yield the fECG [7]. From the estimated fECG component of the fQRS component of the fECG can be easily detected. Similarly to TS, Extended Kalman Filtering (EKF) is a non-linear adaptation of the Kalman Filter that extracts the fQRS by estimating the mECG and subtracting it from the aECG [8]. These methods are well suited for the extraction of the fQRS from noisy aECG [9], but do not demonstrate reliability for deployment for at-home fHR monitoring.

The Lullaby algorithm is proposed as a completely unique fQRS extraction method that is suited for real-time computation on a wearable device. It utilizes the periodic rhythm of the fetal heartbeat as a simple yet novel feature for the extraction of the fQRS. Using simple peak detection and matrix manipulations, the algorithm performs light computations with better accuracy and significantly greater speed than standard methods.

II. MATERIALS & METHODOLOGY

A. Data Set

Lullaby is evaluated on the Physionet 2013 challenge dataset [10] set A which contains 75 1-minute abdominal ECG recordings sampled at 1000 Hz (fs). The data also includes annotations of the fECG taken directly from the fetus using fetal scalp electrodes.

B. Process Flow

Lullaby operates in two phases called the 'Calibration' and 'Real-Time' phases. The calibration phase calculates the prominence and width of the fQRS. The prominence and width of the fQRS calculated in the calibration phase are used as features for fQRS detection in the real-time phase. The real-time phase simulates the extraction of the fQRS in real-time with a 1-second delay from the recording time. These are illustrated in Fig. 1.

C. Preprocessing

The aECG (X_a) can be considered a linear combination of the fECG (X_f), mECG (X_m), and noise (X_n):

$$X_a = X_f + X_m + X_n \tag{1}$$

To maximize the effectiveness of the fQRS extraction, the aECG's baseline wander (BW) and maternal QRS complexes (mQRS) are removed from the signal.

BW is a low frequency noise component that causes the aECG to oscillate along a low frequency sinusoidal wave. To model BW, a 100-point moving average filter is applied to the aECG and then subtracted from the aECG:

$$Y[n] = X_a[n] - \frac{1}{N}\sum_{k=1}^{N} X_a[n - N + k], N \leq 100 \tag{2}$$

where Y represents the aECG with the baseline removed, and N is the number of observable samples.

The mQRS are usually the most prominent morphological feature in the aECG signal, and thereby need to be removed in order to reliably detect the less prominent fQRS. This is done by first re-orienting the mQRS to face upwards:

$$\hat{Y} = \begin{cases} Y, \text{ if } |min(Y)| \leq max(Y) \\ -Y, \text{ if } |min(Y)| > max(Y) \end{cases} \tag{3}$$

A peak finding algorithm is applied which detects the K most prominent peaks in $\hat{Y}$, where K is the duration in seconds of the ECG segment being processed. A secondary peak finding algorithm is applied which detects peaks at a height higher than 75% of the median height of the first set of peaks. This second set of peaks are mostly the mQRS within aECG. The duration of the mQRS complex is on average 100ms, therefore all indexes within 50ms (50 samples) of the mQRS are set to zero. In total these prepossessing steps reduces the aECG signal down to its fECG component.

D. Periodic Trend Feature

The fECG can be approximately modeled as a periodic signal with the fQRS being the repetitive morphology. A period T_o can be used to approximate the separation of the fQRS, and likewise be used to distinguish between true and false fQRS. Consider a B-length vector ψ_B which contains a mix of true and false fQRS indexes in ascending order. By determining the permutation of all delays between the fQRS in ψ_B with respect to T_o, the indexes of true fQRS in ψ_B which best follow the periodic trend T_o are distinguishable:

$$\Psi_{B,B} = \frac{\psi_B - \psi_B^T}{T_o} \tag{4}$$

The row and column of elements of $\Psi_{B,B}$ within 0.15 of an integer value can be used to identify the indexes of ψ_B which correspond to the fQRS as shown in Fig. 2.

To determine the best value of T_o to approximate the fQRS separation, Lullaby tries all integer T_o values. The fHR can be between 80 and 180 bpm. This corresponds to a range of fQRS intervals between 333 ms (333 sample) to 750 ms (750 sample) which can be expressed as a set L:

$$L = \langle 333 \ 334 \ \ldots \ 749 \ 750 \rangle \tag{5}$$

The rows and columns of $\Psi_{B,B}$ lie along the i-th and j-th dimensions respectively. However if $\Psi_{B,B}$ was divided by L along a k-dimension perpendicular to the ij-dimensions, all possible $\Psi_{B,B}$ would be computed in a single 3-D matrix G:

$$G_{k,i,j} = \frac{\psi_B - \psi_B^T}{L_k} \tag{6}$$

To determine which index of G would yield the best $\Psi_{B,B}$ the difference between the elements of G to the nearest integer must be computed and summed along the i-th dimension:

$$\hat{G} = |\lfloor G \rceil - G| \tag{7}$$

$$Z_{k,j} = \sum_{i=1}^{B} \hat{G}_{k,i,j} \tag{8}$$

Elements of Z represent the total deviation of the fQRS from the periodic trend T_o grouped along the i-th dimension. The row (r) and column (c) indexes of the smallest group deviation of Z thereby correspond to the indexes of the best value of T_o and best $\Psi_{B,B}$ column to evaluate along respectively:

$$r, c = \underset{k,j}{\operatorname{argmin}} Z_{k,j} \tag{9}$$

$$W_i = G_{r,i,c} \tag{10}$$

The indexes where W is less than 0.15 correspond to the true fQRS indexes in ψ_B.

E. Calibration

The ‘calibration’ phase (Fig. 3) of Lullaby determines the range of desired widths and prominence that correspond to the fQRS. The process begins by prepossessing the first 12-seconds of the aECG. Peak finding is applied to detect a set of peaks and valley with widths between 5 and $\frac{fs}{35}$. This set is then trimmed down by only keeping peaks and valleys

with prominence greater than $\frac{1}{3}$ of the most prominent peak or valley. Peaks and valleys are finally required to be at least 50 samples apart. The periodic trend feature (PTF) is applied to the remaining peaks to remove the false fQRS. From these calibrated peaks, the upper and bottom bounds of the width feature for the desired fQRS are computed as 2 standard deviations above and below the median width respectively. The same calculations are applied for the prominence.

F. Real-Time

The 'real-time' phase (Fig. 4) of Lullaby extracts the fQRS from the most recent 1 second of data, in-order to simulate real-time extraction. During the real-time phase, the aECG is processed in 4-second batches with the aECG being shifted 1 second in time after each completed cycle. During each cycle, the aECG segment is first preprocessed followed by the application of two peak detection algorithms PDA and PDB. PDA detects all peaks and valleys within the acceptable range of widths and prominence determined in the calibration step with a required separation of 300 samples. PDB detects all peaks and valleys that surpass the lower bounds of the width and prominence only. PDA determines which peak and valley features meet the specifications for the fQRS detected in the calibration step, while PDB attempts to recover fQRS that may have fallen outside those specifications. PTF is applied to PDA with the best period to model the fQRS being T_A. The peaks and valleys detected in PDB that are within $0.75\,T_A$ of a peak or valley in PDA are removed. The remaining peaks and valleys of PDB are inserted into PDA and PTF is recalculated on PDA for the period T_A. The fQRS in PDA within the last 1-second the aECG segment are outputted and the aECG is shifted by 1-second for the next cycle.

G. Evaluation

Lullaby is evaluated on the 'clean' data sets of the Physionet 2013 Challenge Dataset. The chosen records demonstrated a sensitivity score (SE) above 0.5 as calculated by:

$$SE = \frac{TP}{TP + FN} \tag{11}$$

where TP represents the number of true fQRS detected and FN represents the number of true fQRS that were not detected.

The accuracy of the fQRS detection of Lullaby is evaluated cumulatively along the entire aECG using the F1-score:

$$F1 = \frac{2TP}{2TP + FN + FP} \tag{12}$$

where FP are the number of false fQRS that were detected. Additionally, the average computation time for each segment processed during the real-time processing is measured. The computation time is measured from the beginning of the prepossessing step to the determination of the fQRS.

Bland-Altman [11] analysis is used to directly validate the PTF by comparing the average fHR along the entire aECG segment to the average fHR derived by converting all PTFs in processed windows to heart rate and averaging them.

Lullaby was evaluated on a machine with the following specifications: Intel(R) Core(TM) i7-6500U CPU @ 2.50GHz 2 cores 4 logical processors, 16 GB RAM. The Matlab R2021a software was used to conduct the evaluation.

III. RESULTS

Lullaby has an average F1-score of 0.815 on clean data sets and a computation time of 17.8 ms for the real-time phase of the algorithm. Additionally, by determining the memory allocated for the largest data structure we estimate the memory usage to be on average 246.45kB, which can plausibly fit directly on a microcontroller. Compared to ICA, TS, EKF, and their hybrid/modified models [9], Lullaby is approximately 7 times faster than the next fastest algorithm (Table 1). Furthermore Lullaby had a better average F1-score for clean data sets than EKF and ICA, and a comparable score to TS for all data sets (Table 1).

Additionally, the PTF exhibits a fairly accurate representation of the fHR. Bland-Altman analysis (Fig. 5) shows the average PTF deviates from the true heart rate by approximately 8 BPM with 95% confidence and almost zero bias.

IV. DISCUSSION AND CONCLUSIONS

The ongoing COVID-19 pandemic has accentuated the need for home-based fHR monitoring using a wearable device. However, current wearable devices using aECG are unreliable because they either use fQRS extraction algorithms that cannot run in real-time or too computationally heavy to run directly on the wearable device. In this paper, the proposed Lullaby algorithm addresses the former concern while the latter was a design consideration but otherwise will be validated in future works. Comparatively Lullaby is significantly faster than all other comparison algorithms with it being 7 times faster than TS, approximately 17 times faster than RobustICA, approximately 56 times faster than FastICA, and more than 1000 times faster than EKF. In addition, it demonstrated both superior and comparable F1 accuracy to the comparison algorithms.

The novelty of Lullaby stems from the core idea of approximately modelling the fQRS as a periodic occurrence. Using this simple concept, the PTF is able to classify true and false fQRS quickly. Bland-Altman analysis confirms the PTF by itself is able to fairly accurately determine the true fHR within 8 BPM with 95% confidence and no bias. In terms of real-time classification of fQRS in an aECG, PTF demonstrates a strong affinity for the task.

However, for PTF to function the importance of the peak detection steps cannot be discounted. Lullaby heavily uses peak width and prominence features in-order to detect fQRS, which is not a standard method compared to methods such as Pan-Tompkins[12]. The schema is inspired by a similar detection method by Zhang and Yu [13]. Zhang and Yu [13] used the horizontal and vertical distance of peaks as k-means clustering features

for classifying noise, mQRS, and fQRS peaks with an F1-score of 0.9547. The width and prominence feature are inherent to peak finding algorithms and can be used specify peak conditions thereby simplifying the Zhang and Yu implementation [13].

Undeniably, Lullaby is at the forefront of real-time fHR computation and demonstrates a high degree of potential for operation on a wearable device. In future works, the Lullaby algorithm will be implemented on a micro-controller to demonstrate direct computation on a wearable device. We aim to use this opportunity to further quantify its' low-computational complexity with regard to its computation time, power consumption, memory usage for individual functions which cannot be measured appropriately in MATLAB. The accuracy of Lullaby can surely be improved while retaining it's real-time capabilities by optimizing standard methods for real-time implementation and improving detection steps. Although in it's infancy, Lullaby marks the first steps in developing a wearable home-based fHR monitoring system that resolves the aforementioned issues of reliability.

ACKNOWLEDGEMENTS

This work is supported by the NSF CAREER Award 1917105 (H.C.) and the NIH R44 OD024874 (M.P.H.L. and H.C.).

REFERENCES

[1]. Zambrano LD, Ellington S, Strid P, and et al. , "Update: Characteristics of symptomatic women of reproductive age with laboratory-confirmed SARS-CoV-2 infection by pregnancy status — united states, january 22–october 3, 2020," MMWR. Morbidity and Mortality Weekly Report, vol. 69, no. 44, pp. 1641–1647, Nov. 2020. [Online]. Available: 10.15585/mmwr.mm6944e3 [PubMed: 33151921]

[2]. Nageotte MP, "Fetal heart rate monitoring," Seminars in Fetal and Neonatal Medicine, vol. 20, no. 3, pp. 144–148, 2015, fETAL & NEONATAL MONITORING. [Online]. Available: https://www.sciencedirect.com/science/article/pii/S1744165X15000232 [PubMed: 25769203]

[3]. Le T, Moravec A, Huerta M, Lau MP, and Cao H, "Unobtrusive continuous monitoring of fetal cardiac electrophysiology in the home setting," in 2018 IEEE SENSORS, 2018, pp. 1–4.

[4]. Sarafan S, Le T, Ellington F, Zhang Z, Lau MPH, Ghirmai T, Hameed A, and Cao H, "Development of a home-based fetal electrocardiogram (ecg) monitoring system," in 2021 43rd Annual International Conference of the IEEE Engineering in Medicine & Biology Society (EMBC), 2021, Conference Proceedings, pp. 7116–7119.

[5]. Yuan L, Yuan Y, Zhou Z, Bai Y, and Wu S, "A fetal ecg monitoring system based on the android smartphone," Sensors, vol. 19, no. 3, 2019. [Online]. Available: https://www.mdpi.com/1424-8220/19/3/446

[6]. Yuan L, Zhou Z, Yuan Y, and Wu S, "An improved fastica method for fetal ecg extraction," Computational and Mathematical Methods in Medicine, vol. 2018, p. 7061456, 2018. [Online]. Available: 10.1155/2018/7061456 [PubMed: 29887913]

[7]. Lipponen JA and Tarvainen MP, "Advanced maternal ecg removal and noise reduction for application of fetal qrs detection," in Computing in Cardiology 2013, 2013, pp. 161–164.

[8]. Niknazar M, Rivet B, and Jutten C, "Fetal ecg extraction by extended state kalman filtering based on single-channel recordings," IEEE Transactions on Biomedical Engineering, vol. 60, no. 5, pp. 1345–1352, 2013. [PubMed: 23268377]

[9]. Sarafan S, Le T, Naderi AM, Nguyen Q-D, Kuo BT-Y, Ghirmai T, Han H-D, Lau MPH, and Cao H, "Investigation of methods to extract fetal electrocardiogram from the mother's abdominal signal in practical scenarios," Technologies, vol. 8, no. 2, 2020. [Online]. Available: https://www.mdpi.com/2227-7080/8/2/33

[10]. Silva I, Behar J, Sameni R, Zhu T, Oster J, Clifford GD, and Moody GB, "Noninvasive fetal ecg: the physionet/computing in cardiology challenge 2013," Computing in Cardiology, vol. 40, pp. 149–152, 2013. [PubMed: 25401167]

[11]. Bland JM and Altman DG, "Measuring agreement in method comparison studies," Stat. Methods Med. Res, vol. 8, no. 2, pp. 135–160, Jun. 1999. [PubMed: 10501650]

[12]. Pan J and Tompkins WJ, "A real-time qrs detection algorithm," IEEE Transactions on Biomedical Engineering, vol. BME-32, no. 3, pp. 230–236, 1985.

[13]. Zhang Y and Yu S, "Single-lead noninvasive fetal ecg extraction by means of combining clustering and principal components analysis," Medical & Biological Engineering & Computing, vol. 58, no. 2, pp. 419–432, Feb 2020. [Online]. Available: 10.1007/s11517-019-02087-7 [PubMed: 31858419]

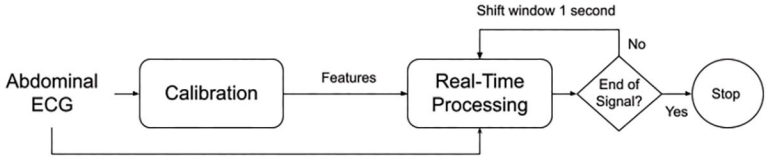

Fig. 1.
Flow chart of Lullaby at a global level.

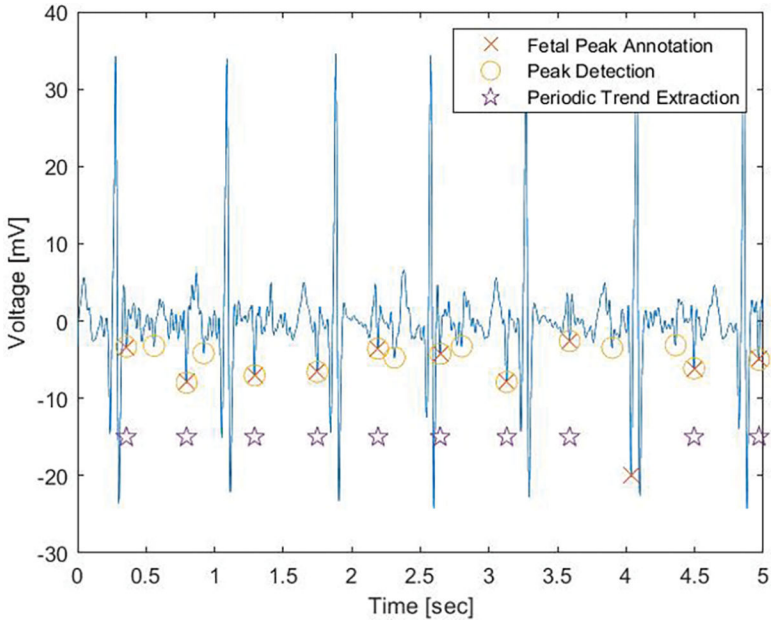

Fig. 2.

An aECG segment with a set of detected peaks containing true and false fQRS. The true fQRS are extracted as the peaks that fit the period T_o = 459 samples.

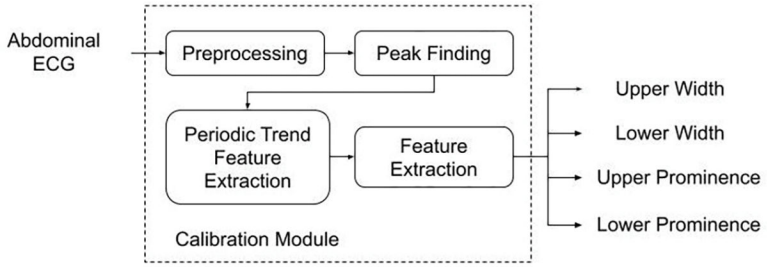

Fig. 3.
Flowchart of the calibration phase of Lullaby.

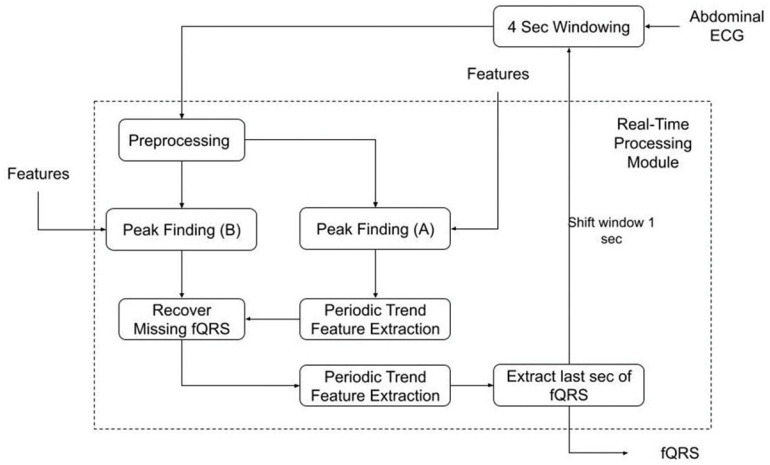

Fig. 4.
Flowchart of the real-time phase of Lullaby.

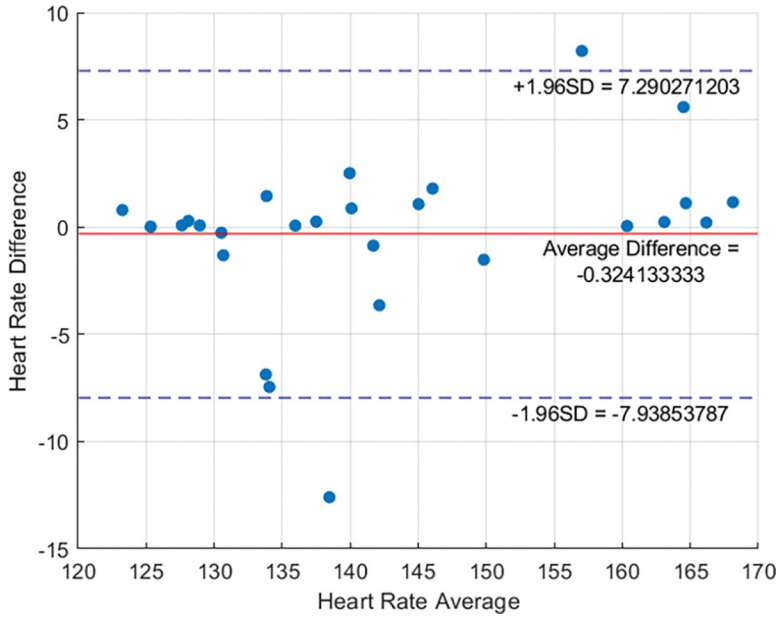

Fig. 5.

Bland-Altman Analysis of average heart rate derived by the true fQRS and the average PTF.

TABLE 1.

Average F1-score and Computation time of Lullaby and standard fQRS extraction methods.

	F1-Score	Computation Time (ms)
Lullaby	0.815	17.8
FastICA	0.6008	~1000
RobustICA	0.5960	~300
TS	0.8265	128
EKF	0.5434	≫1000